McLean seminar

Sec.2.3.2 -2.4.4
2024 4/19 Fri.

Riku Sato (Waseda Univ. Inoue Lab. M2)

Chap. 2 Beating the atmosphere

2.3.2 Fried parameter

- The stellar wavefront incident on a telescope has **spatial variations in amplitude and phase**.
- Regarding to the impact on image quality and seeing.

phase variations > amplitude variations (→scintillation)

- By analyzing the effect of a thin turbulent layer on an incident plane wave, a structure function for phase variations can be derived and integrated throughout the atmosphere.
- The phase structure function $D_\varphi(r)$ across the telescope entrance for **Kolmogorov turbulence** is determined by certain parameters.

$$D_\varphi(r) = 6.88\left(\frac{r}{r_0}\right)^{5/3} rad^2 \qquad (2.4)$$

$$r_0(\lambda, z) = 0.185\lambda^{6/5}\cos^{3/5} z\left(\int C_n^2\, dh\right)^{-3/5} \qquad (2.5)$$

Integrate C^2 [m^(-2/3)] through the atmosphere.
→ r0 [m]

$$r(\lambda) = \left(\frac{\lambda}{\lambda_0}\right)^{6/5} r_0 \qquad (2.6)$$

λ: wavelength, z: zenith distance angle
z = 0 → zenith direction

Fried parameter (r_0) has a larger value at longer wavelengths.

e.g.) 0.5 um (visible light), r_0 ~ 10 cm
→ 2 um (IR), r_0 ~ 50 cm

Fried parameter

・The Fried parameter (r_0) characterizes the size of turbulence cells, representing the **length scale over which the wavefront remains relatively undisturbed.**

・Physical implications of the Fried parameter

1. **It is the aperture size over which there's approximately 1 radian of rms phase error.**
2. **It corresponds to the resolution of a diffraction-limited aperture in the absence of turbulence.**

→ **If r_0 has a larger value, the strength of turbulence is weaker.**

・For instance, if the seeing at the Keck 10m telescope is measured to have an r_0 of 20cm, **the image resolution won't surpass that of a 20 cm telescope.**

→ This is a **serious problem.**

$$r_0(\lambda, z) = 0.185\lambda^{6/5} \cos^{3/5} z \left(\int C_n^2 \, dh \right)^{-3/5} \qquad (2.5)$$

Coherence time

- Turbulent elements responsible for seeing last longer than the transit time across their diameters, making wind velocities across different atmospheric heights crucial for temporal variations in the wavefront.

$$\tau_0 \approx 0.314 \frac{r_0}{v} \qquad (2.7)$$

- Temporal variations across the wavefront are typically on the order of milliseconds, influenced by wind velocities averaging around 10 m/s.
- The Greenwood frequency $f_G \sim 0.43 v/r_0$ indicates the rate at which corrections are needed due to turbulence, typically around 43 Hz for the discussed values.
- Motion in the image plane is independent of wavelength.
- **We can estimate needed time scale for compensation cycles from coherence time.**

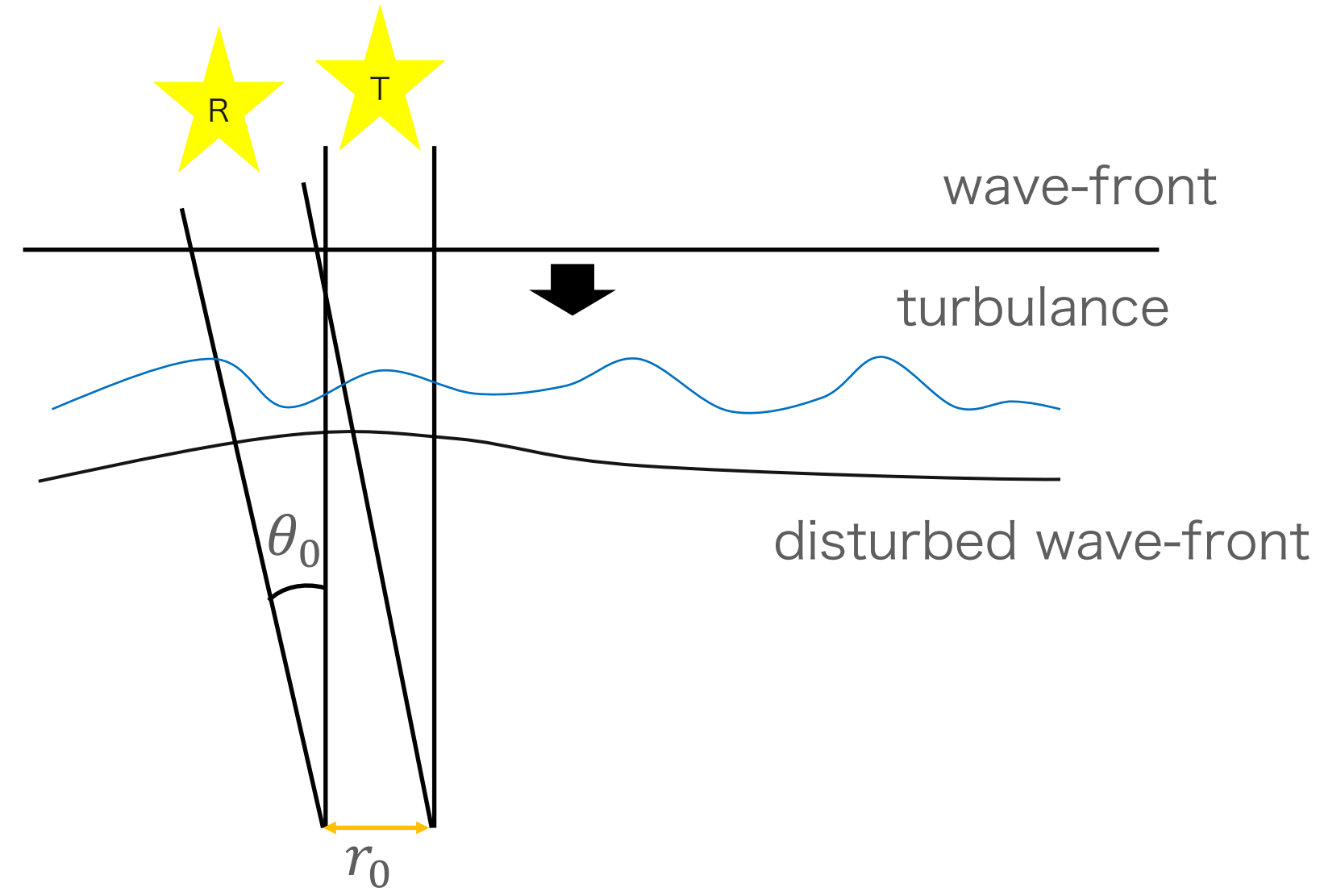
R
T
wave-front
turbulance
disturbed wave-front
θ_0
r_0

"knife-edge" observation

- Using a sharp "knife-edge" halfway across and precisely in the focal plane of the telescope allows obscuring part of the seeing disk of a star.
- This setup enables observers to look back into the telescope and view the illumination of the primary mirror. Observers can detect the direction, speed, and size of the changing pattern of turbulent cells.
- The resulting image, known as the Schlieren pattern, appears turbulent and is composed of changing light and dark patches.
- Horace W. Babcock conducted pioneering studies of this phenomenon from about 1936 onwards, making hundreds of visual knife-edge observations at various observatories, measured r_0 at various sites.
- **The value of r_0** is observed to be **site-dependent** and also **wavelength-dependent, slightly better in the infrared.**
- r_0 values range from a few centimeters to as large as **100 cm at wavelengths of 2.2 mm, reported for Mauna Kea**.
- **For very large telescopes (8m-10m), even an r_0 of 1 m is considered too small.**

Speckle

- If the exposure time is shorter than τ_0 which is the time taken for one cell of turbulence to move a distance r_0 across the primary mirror diameter (D).
- **The total number of speckles ~** $(D/r_0)^2$.
- **The width of each speckle ~** λ_0/D.
- Numerous short exposures, when added together or equivalently represented by a long exposure, result in the blending of the displaced speckles.
- This blending creates a broad seeing disk with a width of λ_0/r_0 (= seeing size, PSF FWHM blurred by turbulance), rather than a sharp image with a diffraction-limited width of λ_0/D.
- **The Fried parameter r_0 defines the equivalent diffraction-limited aperture,** typically corresponding to **a value at a wavelength of λ_0 = 500 nm.**
- **A larger r-naught corresponds to fewer speckles, better long-exposure seeing, longer coherence time, and a larger Strehl ratio.**

→ better at longer wavelengths

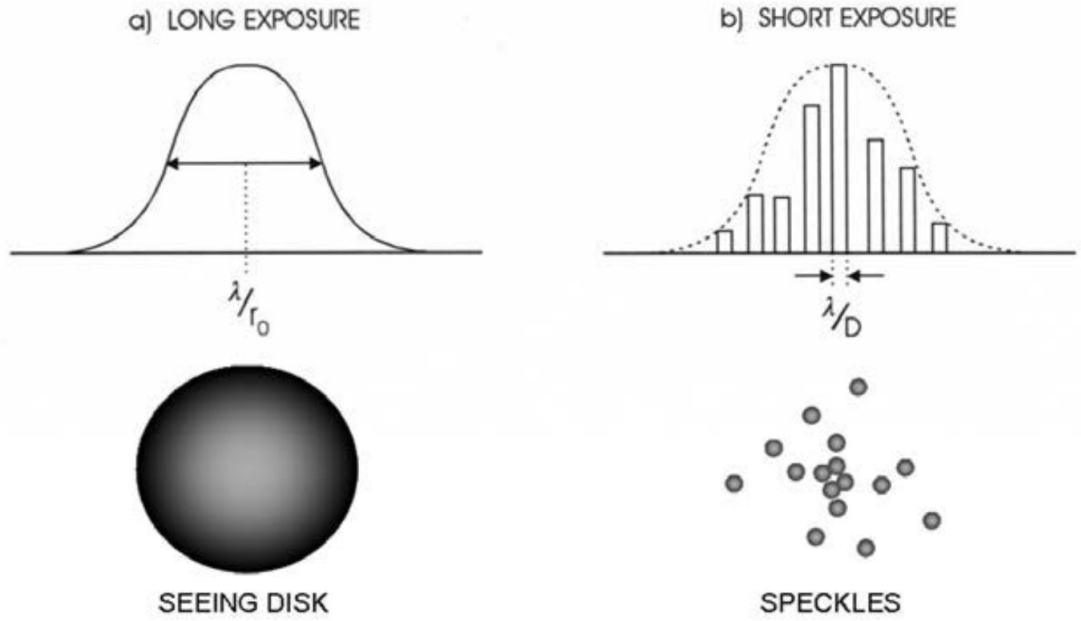

exposure time < τ_0 → We see speckles.
exposure time > τ_0 → Speckles blur into a seeing disk.

$$\tau_0 \approx 0.314 \frac{r_0}{v} \qquad (2.7)$$

2.3.3 Speckle interferometry

- **Speckle interferometry**, pioneered by French astronomer **Antoine Labeyrie** in the 1970s**, reconstructs the diffraction-limited image** from the analysis of **numerous short speckle images** using **Fourier analysis** techniques.
- requires **short exposures**, which demand **high detector performance** due to limitations imposed by **readout noise**.
- speckle interferometry has proven to be effective, as demonstrated by observations of **close binary stars** by Andrea Ghez (UCLA) using an infrared speckle camera at a wavelength of 2.2 mm.
- The power spectra, or square of the Fourier amplitudes, reveal **fringe patterns whose spacing decreases with increasing binary separation.**
- Reconstruction of images from speckle patterns involves **inverse Fourier transform** of the amplitudes and phases of the speckle pattern, enabling the construction of detailed images.
- Further discussion on image reconstruction and Fourier techniques is provided in Section 10.4.

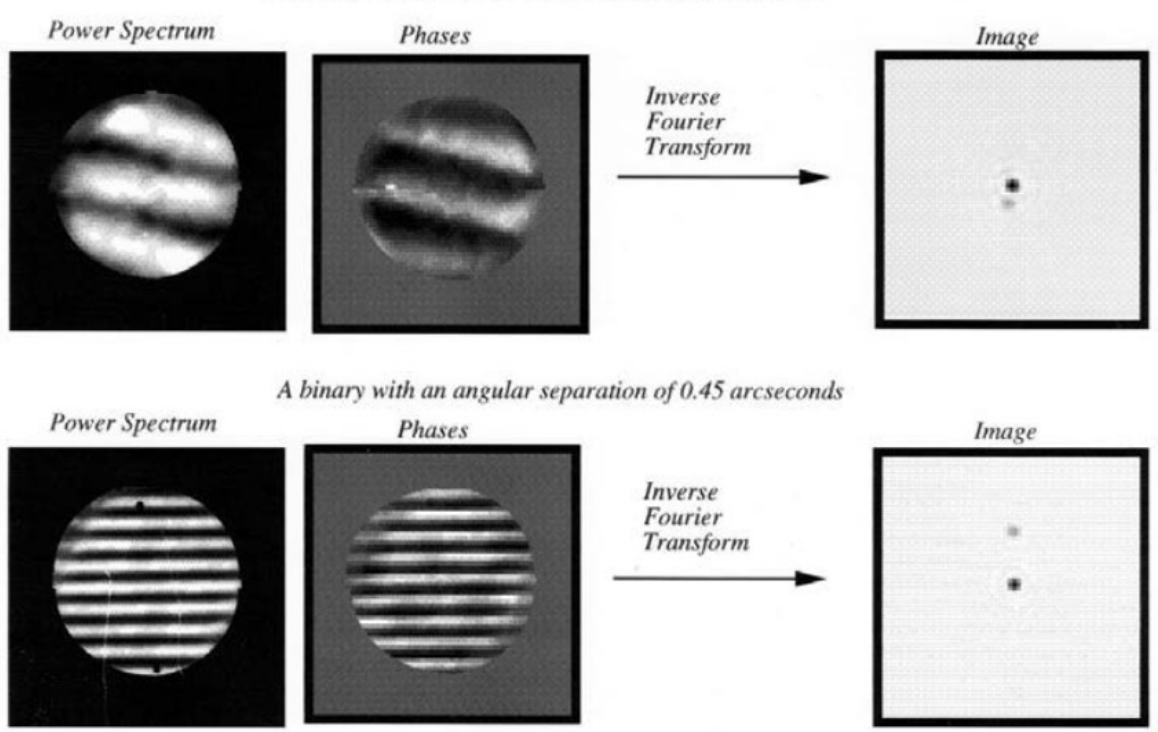

2.3.4 Lucky imaging

・A simpler strategy involves recording snapshots and using computer processing to "shift-and-add" each image. This process aligns the brightest speckles in each snapshot, but detector noise remains an issue.

・An extension of this idea is "lucky imaging" which selects only the best short exposures for processing into the final image.

・"lucky imaging" is not limited to bright objects; utilizes extremely sensitive CCDs with pixels acting as "avalanche" photodiodes

→ produces a large "gain" (like a photomultiplier tube)

→ a faint photon signal becomes a strong photo-electron signal that overcomes the intrinsic readout noise of the CCD.

・These CCDs, also known as electron-multiplied (EM) or "low light level" (L3CCDs), are made by e2v technologies.

・Merit: excellent images by capturing moments of excellent seeing.

・Demerit: need to reject a large fraction of the snapshots.

・This approach will be revisited in Section 7.5.1.

tip-and-tilt motion

More general way to undo the effect of r_0?

First step

compensating for the random wandering of the centroid of the seeing disk through tip-and-tilt (x-y) motion of a mirror, potentially the secondary mirror of the telescope, to direct the overall wavefront to a fixed position in the image.

Detect wavefront distortion

Second step

- An optical arrangement is used to project a real, de-magnified image of the primary mirror of the telescope onto a much smaller mirror whose detailed "shape" can be changed or "deformed" by the forces applied from **numerous small actuators** behind it.
- **A high-speed CCD camera functions as a wavefront sensor**, rapidly detecting changes in the slope of coherent areas of turbulence, referred to as sub-apertures.
- By analyzing the wavefront distortions, corrections are made to the **deformable mirror (DM)** to compensate for the distortions, effectively restoring the wavefront.

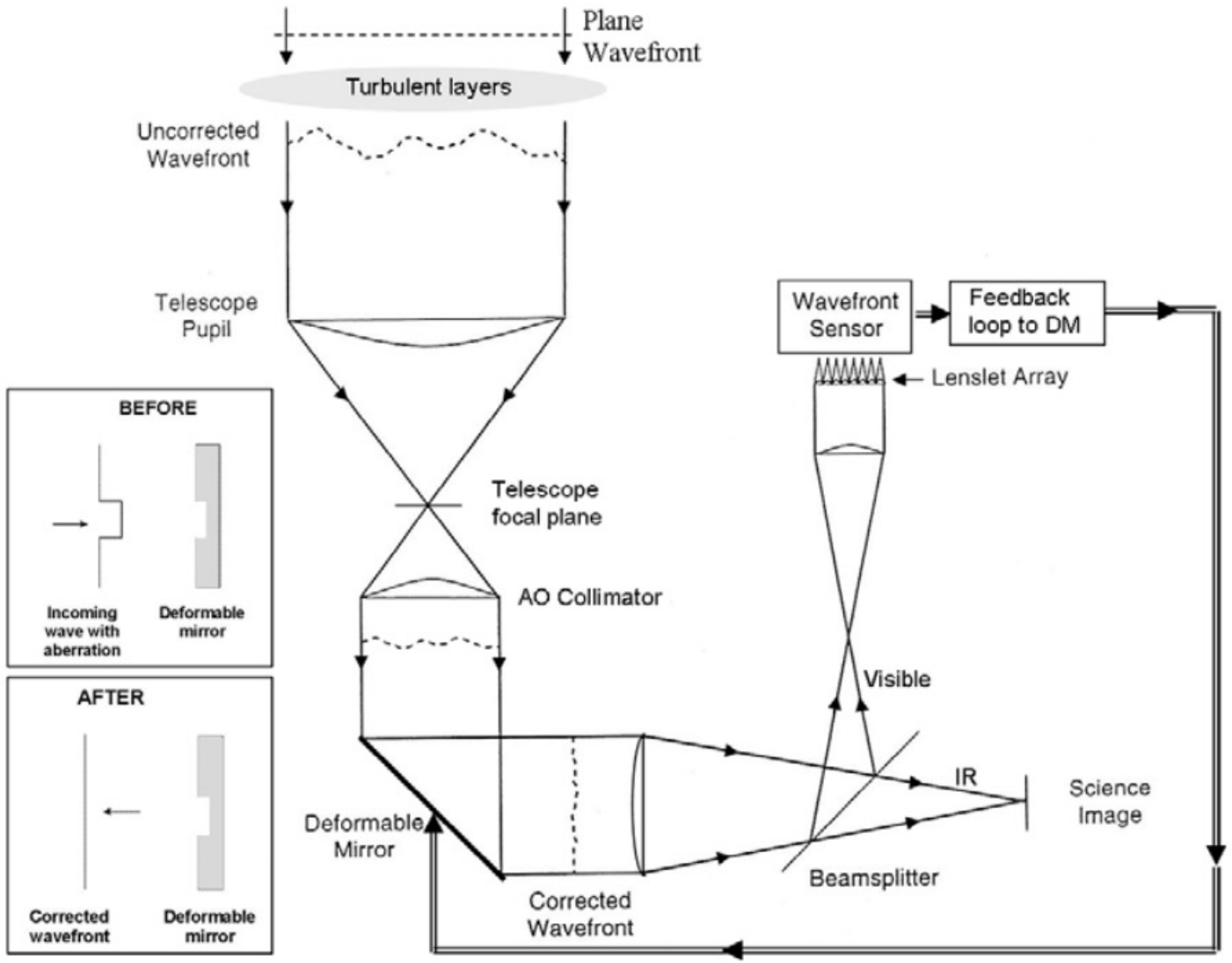

Deformative mirror

- The disturbed wavefront enters the telescope aperture and is re-imaged onto the **DM.**
- If the otherwise plane mirror is deformed to have half the wavefront error of the incoming wave, the reflected wavefront will be nearly a plane wave after leaving the DM.
- This is because the corresponding part of the wave must travel into and out of the depression in the DM, aligning with the rest of the wave upon reflection.
- Correction signals from the wavefront sensor are used to adjust the deformable mirror, closing the loop and refining the correction process.

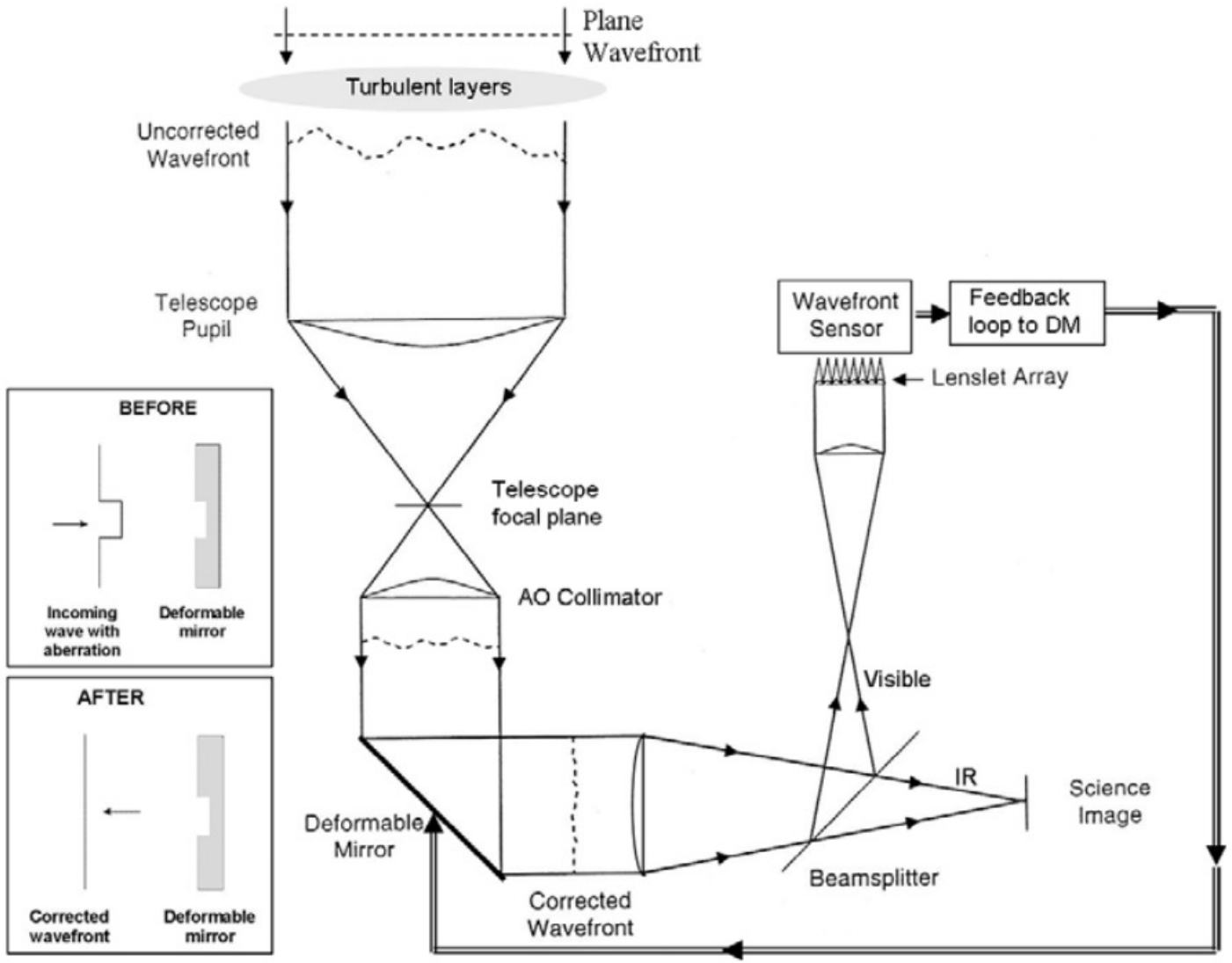

Wavefront sensors

Two groups

Direct sensors split the pupil image plane into sub-apertures and use the intensity in each sub-aperture to deduce the phase of the wavefront.

→two sub-categories

- slope-sensing: Shack-Hartmann
- curvature-sensing: shear interferometer, and (more recently) pyramid sensors.

Indirect sensors deduce wavefront properties from whole-aperture intensity measurements made at or near the focal plane. These methods include image sharpening, multi-dither, phase diversity, and phase retrieval. Techniques that use sub-apertures place greater demands on the CCD detector because less light is collected for each sub-aperture.

Shack-Hartmann wavefront sensor system

Shack-Hartmann slope-sensing type with many sub-apertures.

- an array of tiny lenses or "lenslets" which is placed near a pupil image to produce a pattern of many star images on the detector, each corresponding to a different part of the primary aperture.
- The slopes of the wave-fronts incident on each lens make images displaced from the nominal positions.

→ By rapidly finding the centroids of each image it is possible to derive the slope of the wavefront at that instant.

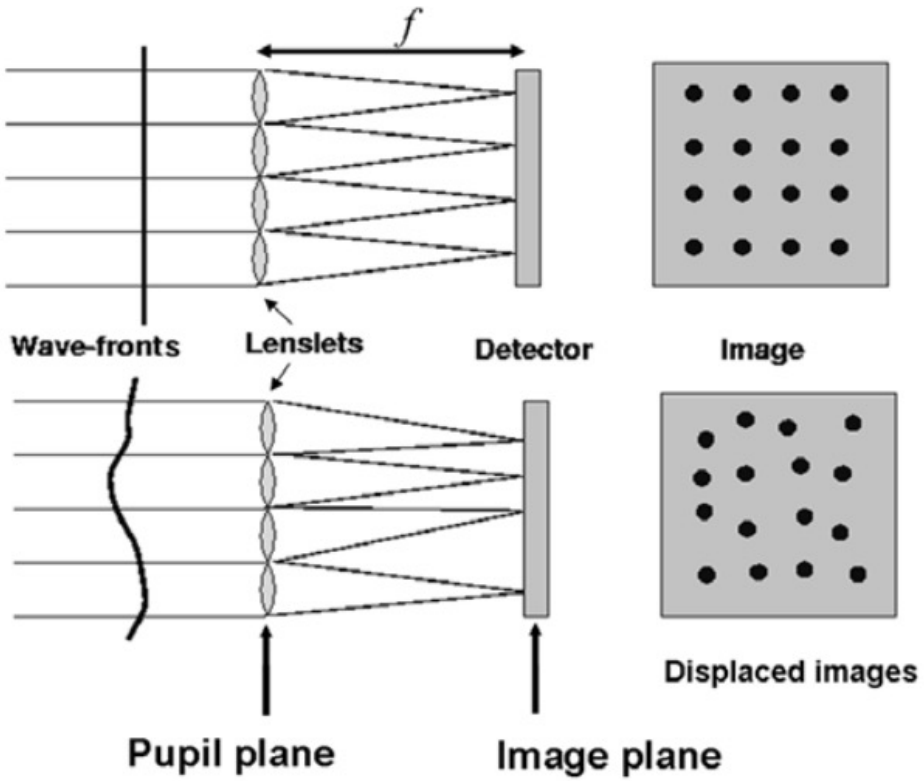

Shack-Hartmann wavefront sensor system

e.g.) Keck 10 m telescope the pupil image on the lenslet array is reduced in size by a factor of 2800 from 10 m.

- The lenslet array = approximately 18 x 18 lenses (each about 200 um in diameter)

→ total size: about 3.6 mm on a side.

- 200 um sub-aperture corresponding to the huge size on the primary mirror.

→ the lenslet diameter 200 um x the magnification factor of 2800 = 56 cm

~ expected value of the Fried parameter in the range of 1 um to 2 um.

→ a smaller light-gathering area for the wavefront sensor.

Shack-Hartmann wavefront sensor system

・lenslet size (200 um) > a typical CCD pixel (~20 um)

→ normal lenses are required in front of the CCD to reduce the scale.

・Each spot on the CCD might be matched to a 3x3 grid of pixels, with the inner 2x2 forming a "quad-cell" arrangement.

・Displacement in the x and y directions can be determined by comparing intensity differences between quadrant pairs and dividing by the total intensity, then multiplying by the radius of the spot image.

・If the sub-aperture size is approximately equal to r, the wavefront error (WFE) can be roughly estimated as 6.3/SNR (radians) (SNR = signal-to-noise ratio).

・To ensure the WFE is less than $\lambda/20$ or $\lambda/10$ radians, the SNR should be greater than 20.

・Typically, small high-speed CCDs with frame rates of a few thousand per second, high quantum efficiency (approximately 80%), and low noise (around 3 electrons) are required.

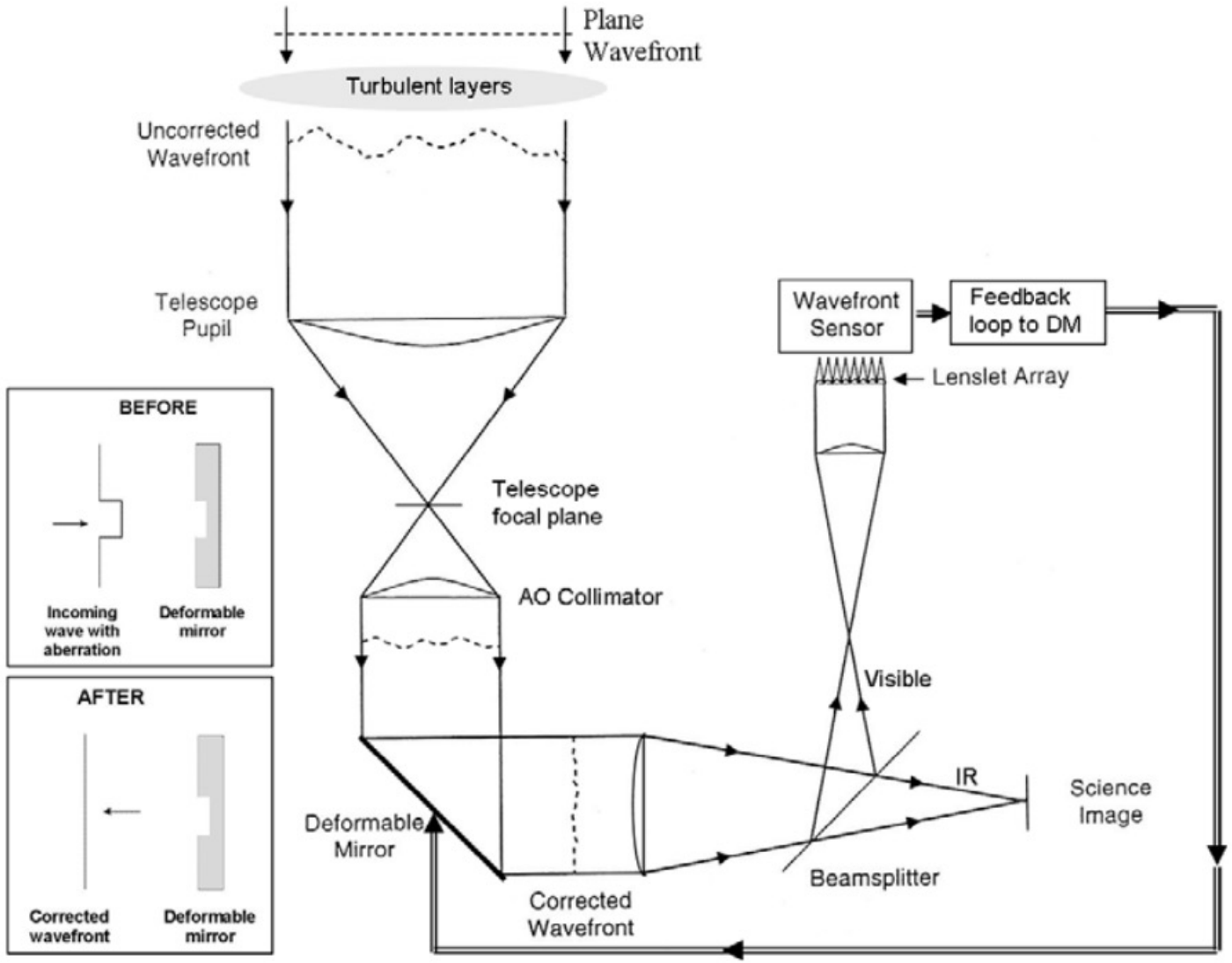
Plane
Wavefront
Turbulent layers
Uncorrected
Wavefront
Telescope
Pupil
Wavefront
Sensor
Feedback
loop to DM
Lenslet Array
BEFORE
Incoming
wave with
aberration
Deformable
mirror
Telescope
focal plane
AO Collimator
AFTER
Corrected
wavefront
Deformable
mirror
Visible
IR
Science
Image
Deformable
Mirror
Beamsplitter
Corrected
Wavefront

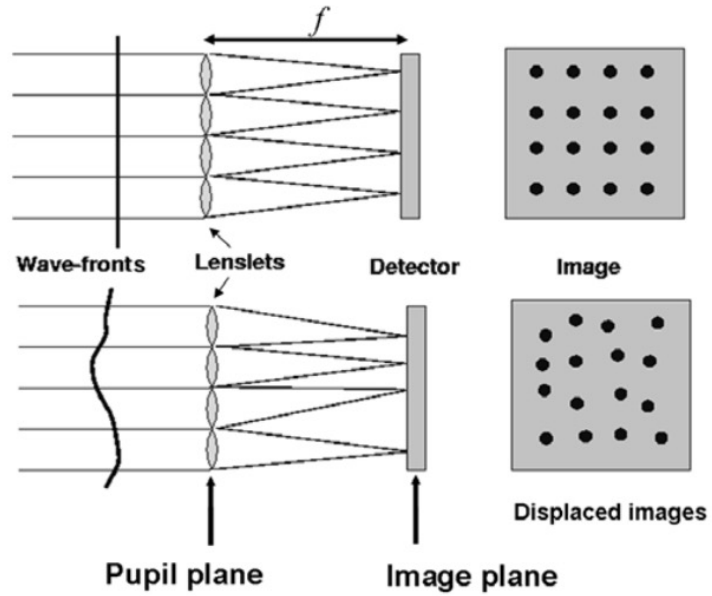
f
Wave-fronts
Lenslets
Detector
Image
Displaced images
Pupil plane
Image plane

Zernike polynomials

Phase variations in the wavefront are described using **Zernike polynomials $Z_j(n,m)$.**

Low-order Zernike terms and their meanings, along with the mean square residual amplitude in phase variations at the telescope entrance caused by Kolmogorov turbulence after removal of the first j terms.

Table 2.1. Modified Zernike polynomials and the mean square residual amplitude for Kolmogorov turbulence after removal of the first j terms.

Z_j	n	m	*Expression*	*Description*	Δ_j/S
Z_1	0	0	1	Piston	1.030
Z_2	1	1	$2r\sin\varphi$	Tilt	0.582
Z_3	1	1	$2r\cos\varphi$	Tilt	0.134
Z_4	2	0	$\sqrt{3}(2r^2-1)$	Defocus	0.111
Z_5	2	2	$\sqrt{6}r^2\sin 2\varphi$	Astigmatism	0.0880
Z_6	2	2	$\sqrt{6}r^2\cos 2\varphi$	Astigmatism	0.0648
Z_7	3	1	$\sqrt{8}(3r^3-2r)\sin\varphi$	Coma	0.0587
Z_8	3	1	$\sqrt{8}(3r^3-2r)\cos\varphi$	Coma	0.0525
Z_9	3	3	$\sqrt{8}r^3\sin 3\varphi$	Trifoil	0.0463
Z_{10}	3	3	$\sqrt{8}r^3\cos 3\varphi$	Trifoil	0.0401
Z_{11}	4	0	$\sqrt{5}(6r^4-6r^2+1)$	Spherical	0.0377

trefoil?

$$\Delta_j \approx 0.2944 j^{-0.866}\left(\frac{D}{r_0}\right)^{5/3} rad^2 \qquad (2.8)$$

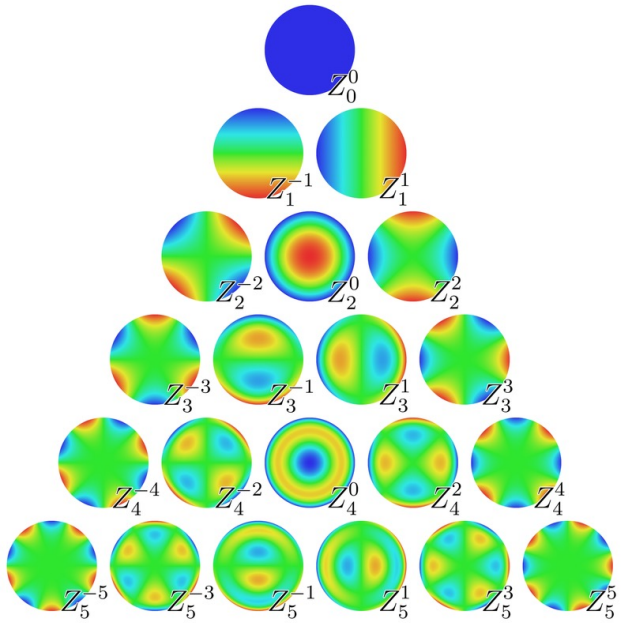

https://ja.wikipedia.org/wiki/ゼルニケ多項式

Zernike polynomials

- **Phase variations in the wavefront** are described using **Zernike polynomials** $\boldsymbol{Z_j(n,m)}$, where **n represents the degree of a radial polynomial** and **m is the azimuthal frequency of a sinusoidal term**.
- This description allows aberrations in the wavefront to be visualized similarly to **how the surface of a deformable mirror will be treated.**
- **Ray-tracing programs can provide theoretical wavefront patterns in terms of Zernike polynomials, aiding in the assessment of lens effects.**
- Noll (1976) provides normalized versions of Zernike polynomials where the root mean square (rms) value of each polynomial over the circle is unity.

Shack-Hartmann wavefront sensor system

- The rms phase variation for each mode of correction can be calculated by substituting the appropriate terms and taking the square root.
- With no wavefront correction, the rms phase variation is relatively high.
- After tip/tilt correction, the rms phase variation decreases significantly.
- With further correction, such as adaptive optics, the rms phase variation is further reduced.
- The Strehl ratio (SR) is an important metric for assessing image quality, with higher values indicating better performance.

$$SR = \text{(observed peak intensity)/(ideal peak intensity)}$$

- Achieving a high Strehl ratio $SR > 0/8$, especially for very large telescopes under average seeing conditions, requires a significant number of Zernike terms and actuators on the deformable mirror.

$$1 - SR \approx \Delta \approx 1 - e^{-\Delta} \qquad (2.9)$$

2.4.2 The isoplanatic patch

・The correction process has several limitations.

1. A bright star is used as a reference to provide a good SNR in each sub-aperture across the primary mirror. Generally, the target object being observed is too faint to serve as its own reference.

2. **Compensation effectiveness decreases with angular distance from the reference star** because **wavefront distortions vary**.

→**Perfect compensation is limited** to **an angular patch** around **the reference star,** known as **the isoplanatic region.**

・**The isoplanatic angle** is defined as **the radius of a circle** over which **wavefront disturbance is essentially identical**.

$$\theta_0 = 0.314 \frac{r_0}{H} \qquad (2.10)$$

2.4.2 The isoplanatic patch

The term "isokinetic patch" can also be used to refer to the angular distance over which image motions are practically the same as compared with seeing widths.

$$\text{isokinetic patch} = 0.3\frac{D}{H}$$

e.g.) an 8 m telescope, r_0 = 13.3 cm (a seeing of 0.75 arcsec at 500 nm), the seeing layer (H) of 5000 m

→ The radius of isoplanatic patch = 8 x 10^(-6) [rad] ~ 1.7"

< The isokinetic patch = 5 x 10^(-4) [rad] ~ 100"

$$\theta_0 = 0.314\frac{r_0}{H} \qquad (2.10)$$

2.4.3 Deformable mirrors (DMs)

・Segmented DMs: Each segment has 1-3 actuators and can correct in-out motion (piston) and tip-tilt.

・Continuous Face-Sheet DM: Use a thin "face" sheet of low-expansion glass supported on an array of many small, discrete actuators, typically over 900 actuators.

・Bimorph DMs: Consists of two piezoelectric wafers bonded together with an array of electrodes between them; the front surface acts as the deformable mirror.

・Micro-Electro-Mechanical Systems (MEMS): Fabricated using silicon micromachining, and actuation of the membrane mirror is by electrostatic forces.

→1000 actuators with 2um stroke. 4000 actuator devices were developed?

・Liquid Crystal Devices

AO188 at Subaru telescope uses 188-element bimorph-type DM.

2.4.3 Deformable mirrors (DMs)

Types of deformable mirrors (DMs)

- segmented
- continuous face-sheet
- bimorph
- Micro-Electro-Mechanical Systems (MEMS)
- liquid crystal devices.

Continuous face-sheet DM

↑ Keck Observatory

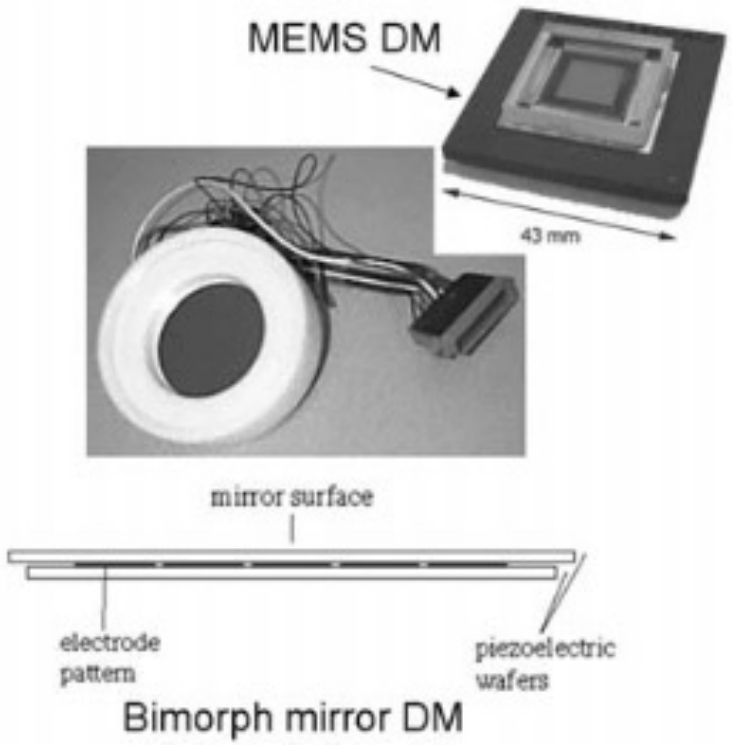

Bimorph mirror DM

2.4.3 Deformable mirrors (DMs) as secondary mirror

- 6.5m Monolithic Mirror Telescope (MMT) on Mt. Hopkins (Arizona)
- >300 magnetically activated force actuators
- In operation this system yields a factor-of-20 improvement of the Strehl ratio at the operating wavelength of 1.65 mm.
- A larger system is planned for the Large Binocular Telescope on Mt. Graham (Arizona).

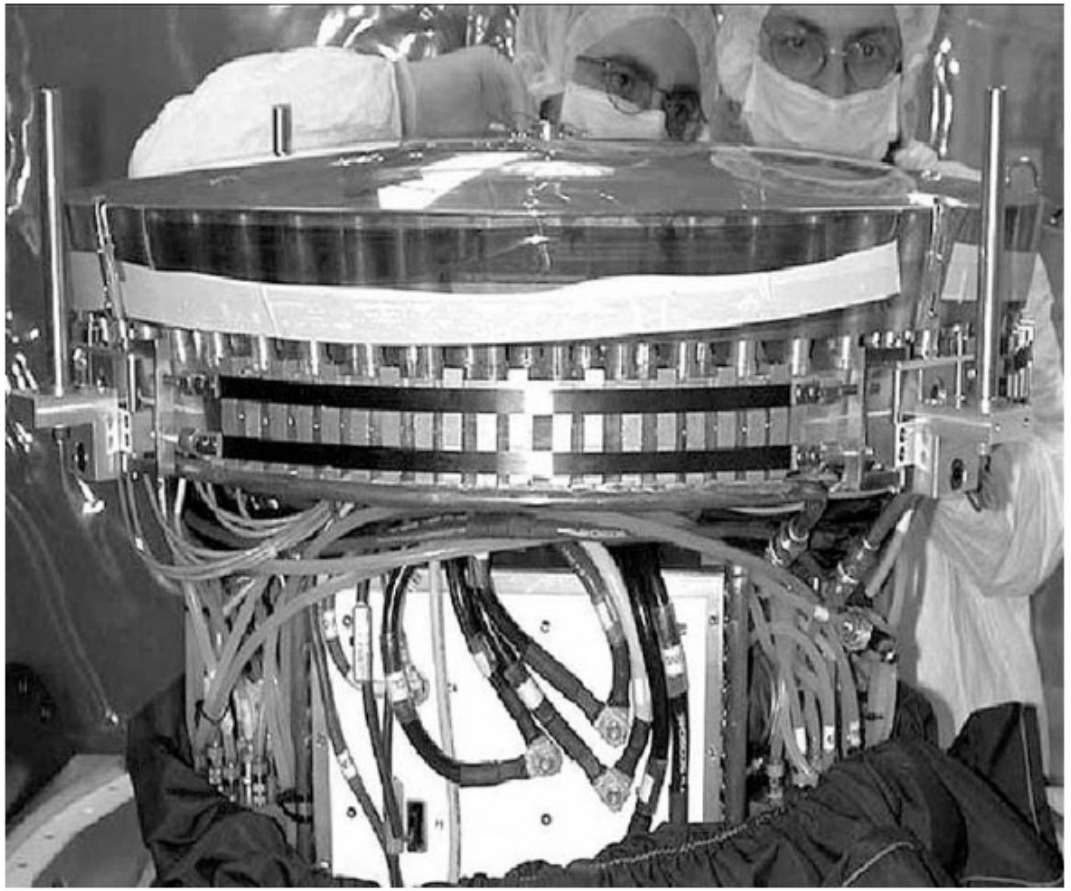

2.4.4 Natural guide star systems

In the late 1980s, observatories began developing adaptive optics (AO) systems, recognizing the potential for correcting atmospheric distortions in the visible spectrum, which also benefitted near-infrared instruments. Some notable developments include:

- Come-On System for ESO 3.6m telescope
- Nasmyth Adaptive Optics System (NAOS) for VLT
- Lawrence Livermore National Labs (LLNL) System for Lick observatory
- AO for Canada-France-Hawaii Telescope (CFHT)

2.4.4 Natural guide star systems

Come-On System: Developed by Observatoire de Meudon (France) and European Southern Observatory (ESO) for the ESO 3.6 m telescope in Chile, later upgraded to Adonis. It featured a deformable mirror with 19 piezoelectric actuators and a Shack-Hartmann wavefront sensor with 5x5 sub-apertures. The infrared science camera had 32x32 pixels.

Nasmyth Adaptive Optics System (NAOS): Collaborative effort between ESO and a French consortium for the Very Large Telescope observatory at Paranal in Chile. NAOS had the option to use an infrared wavefront sensor.

2.4.4 Natural guide star systems

- Lawrence Livermore National Labs (LLNL) System: Developed under the leadership of Claire Max and Scott Olivier, a prototype was deployed at the University of California's Lick Observatory in 1996. It featured a Shack-Hartmann wavefront sensor with a triangular array of 37 sub-apertures and a deformable mirror with 127 PMN actuators.
- AO for Canada-France-Hawaii Telescope (CFHT) : Led by François Roddier, CFHT focused on curvature sensing, bimorph mirrors, and avalanche photodiodes (APDs) for high sensitivity.

Since these early efforts for developing natural guide star AO, AO technology has advanced significantly, with improvements in computers and actuators. Dozens of fully operational AO systems are now in use on telescopes of all sizes.

Lick AO

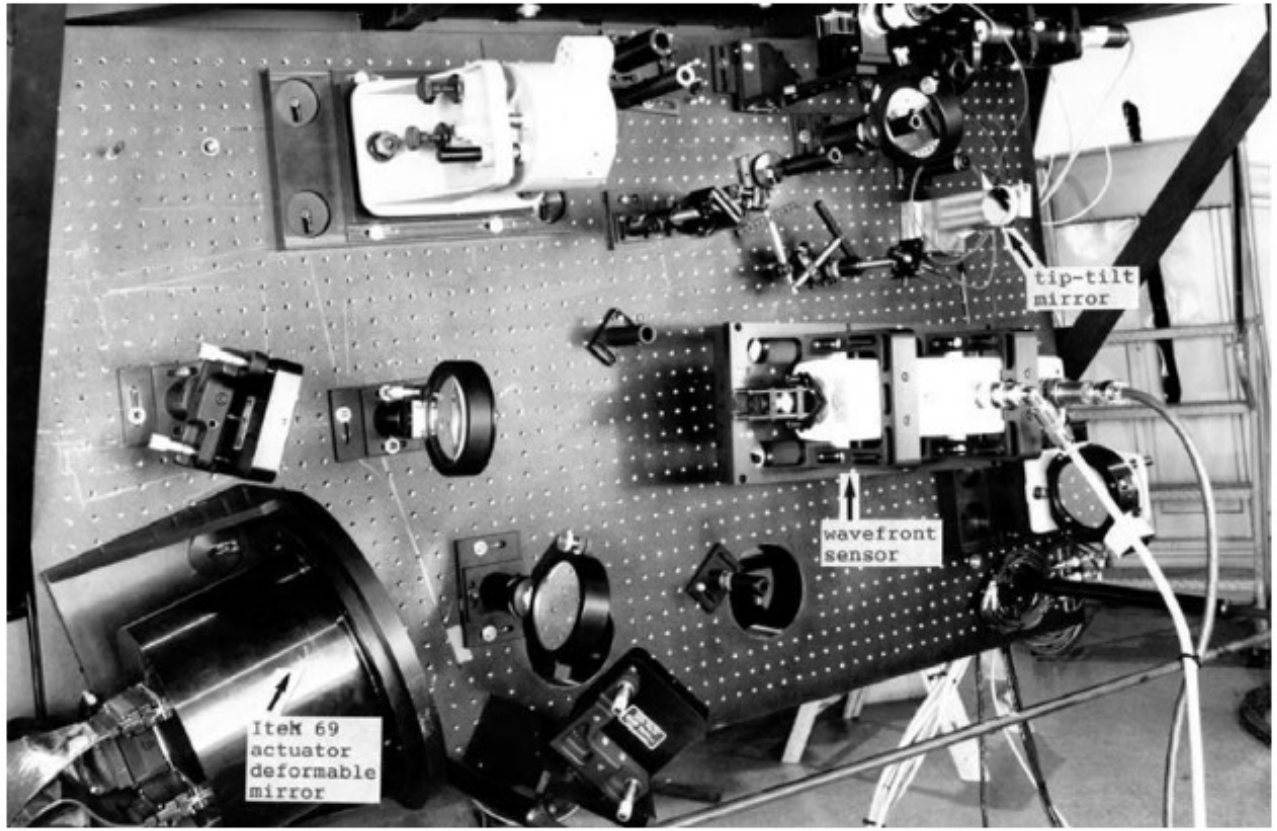
tip-tilt
mirror
wavefront
sensor
ITEM 69
actuator
deformable
mirror

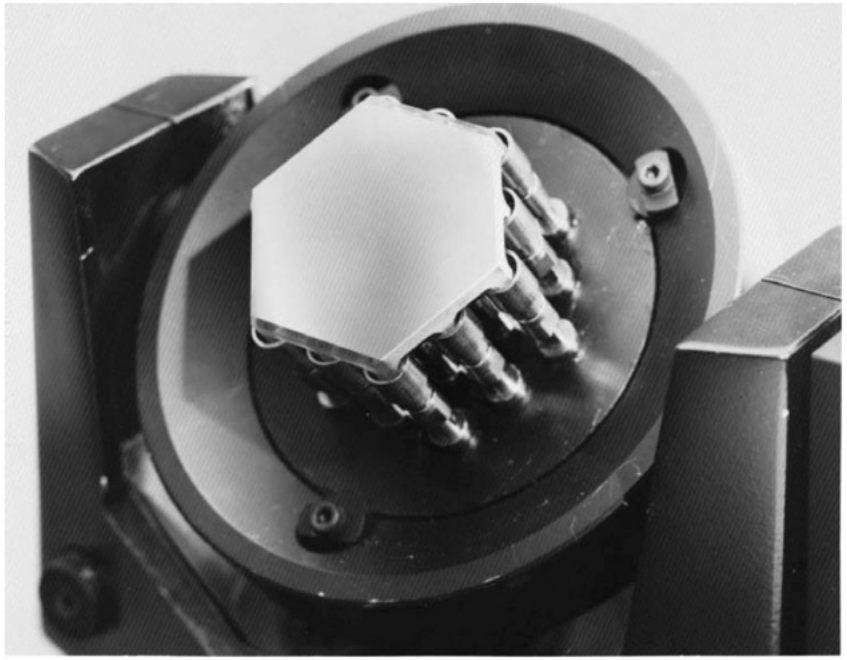

AO188

https://www.naoj.org/Observing/Instruments/AO/system.html

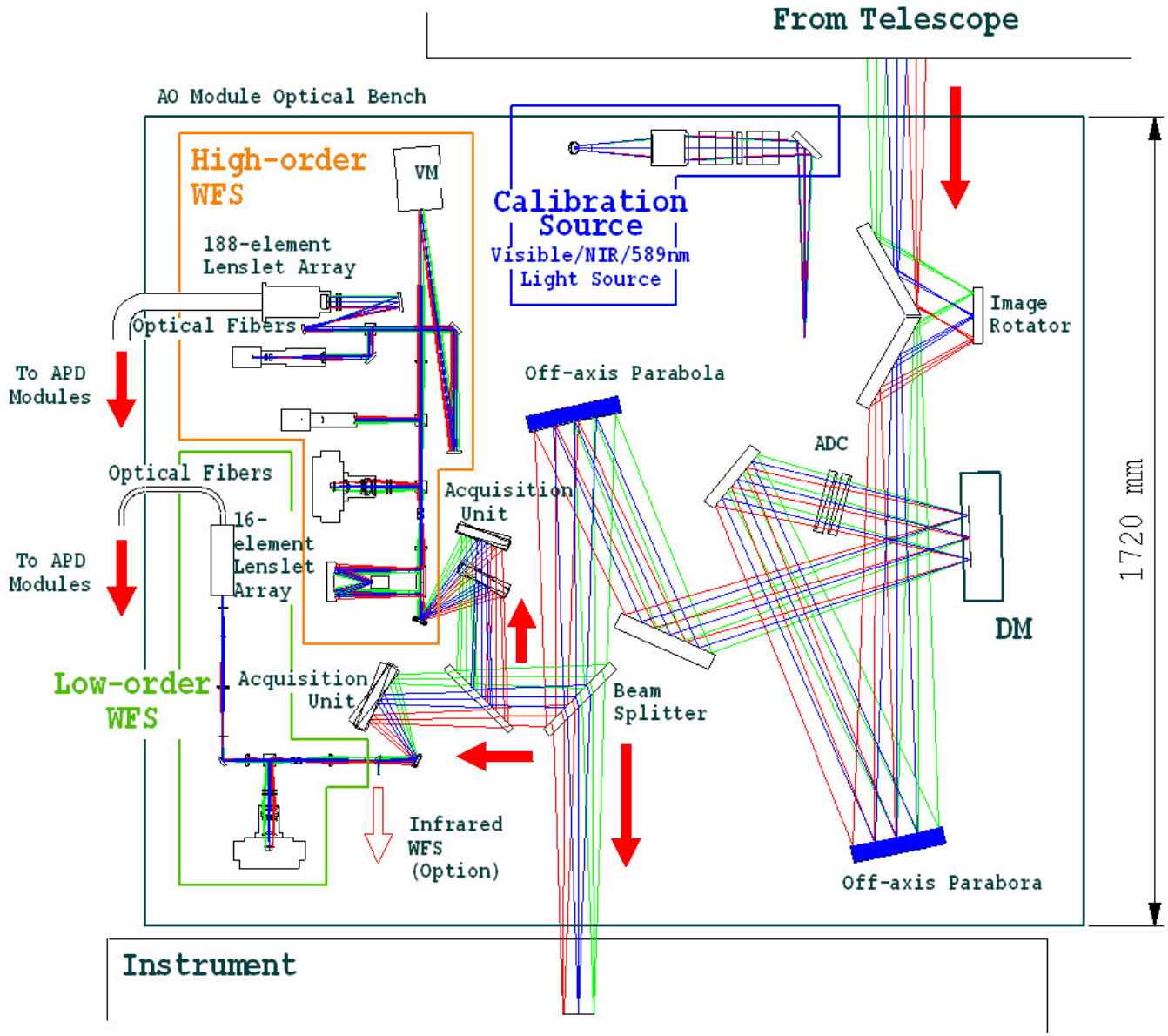

Supplemental material

- Babcock, H. W. (1990)

•Placing a knife-edge in the focal plane of a telescope obscures part of the seeing disk.
•With the observer's eye close behind, the primary mirror can be observed as illuminated by a star.
•This setup reveals the changing pattern of coherent areas resulting from distorted wavefronts.
•By using the knife-edge in various position angles, unwanted distortion of the primary mirror due to flexure or thermal effects can be detected.

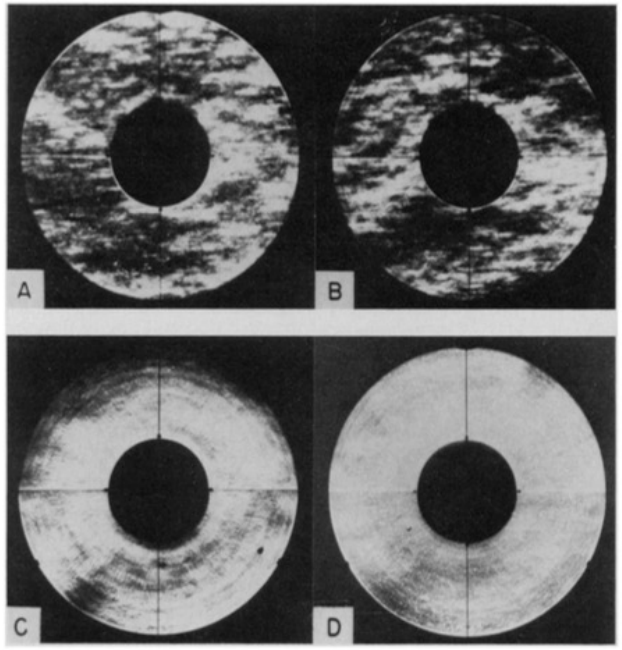

Hale telescope
~ 200inch = 508cm

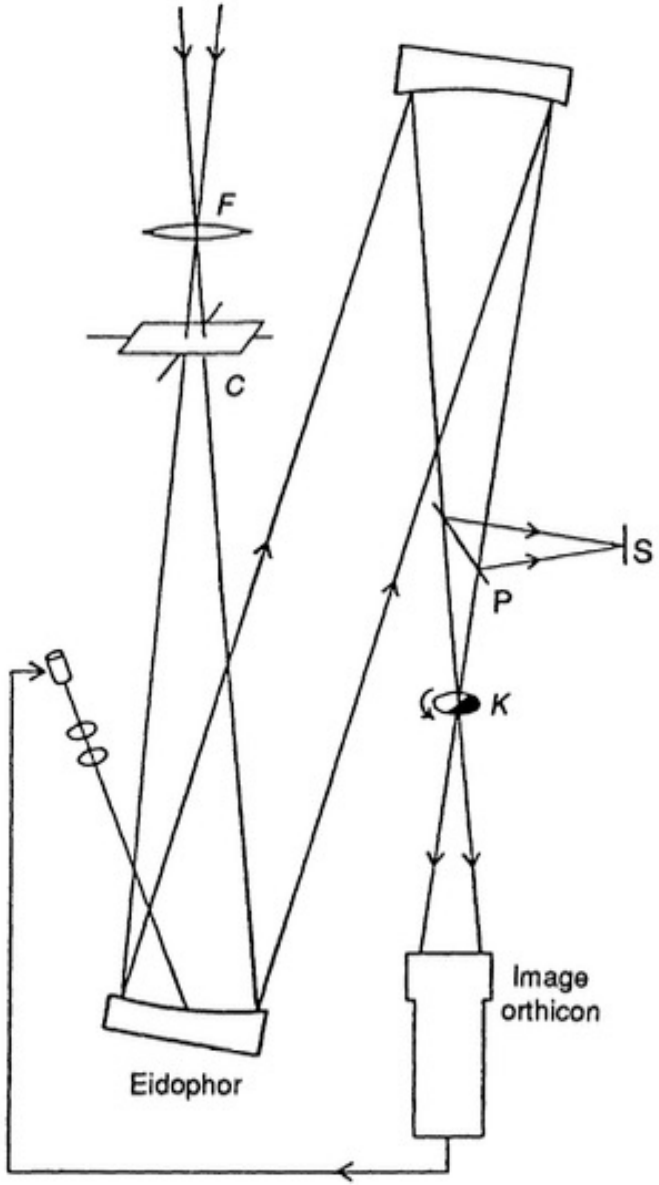

References

- Babcock, H. W. (1990). Adaptive Optics Revisited. Science, 249(4966), 253–257. http://www.jstor.org/stable/2874621